

Compton scattering from ^{12}C using tagged photons in the energy range 65–115 MeV

L. S. Myers,^{1,*} K. Shoniyozov,² M. F. Preston,³ M. D. Anderson,⁴ J. R. M. Annand,⁴
 M. Boselli,^{4,†} W. J. Briscoe,⁵ J. Brudvik,⁶ J. I. Capone,^{5,‡} G. Feldman,⁵ K. G. Fissum,^{3,§}
 K. Hansen,⁶ S. S. Henshaw,^{7,¶} L. Isaksson,⁶ R. Jebali,⁴ M. A. Kovash,² K. Lewis,^{5,**} M. Lunding,⁶
 I. J. D. MacGregor,⁴ D. G. Middleton,^{8,††} D. E. Mittelberger,^{5,‡‡} M. Murray,⁴ A. M. Nathan,¹
 S. Nutbeam,⁴ G. V. O’Rielly,⁹ B. Schröder,^{3,6} B. Seitz,⁴ S. C. Stave,^{7,§§} and H. R. Weller⁷

(The COMPTON@MAX-lab Collaboration)

¹*Department of Physics, University of Illinois at Urbana-Champaign, Urbana, IL 61801, USA*

²*Department of Physics and Astronomy, University of Kentucky, Lexington, KY 40506, USA*

³*Department of Physics, Lund University, SE-221 00 Lund, Sweden*

⁴*School of Physics and Astronomy, University of Glasgow, Glasgow G12 8QQ, Scotland UK*

⁵*Department of Physics, The George Washington University, Washington, DC 20052, USA*

⁶*MAX IV Laboratory, Lund University, SE-221 00 Lund, Sweden*

⁷*Department of Physics, Duke University, Durham, NC 27708, USA*

⁸*Kepler Centre for Astro and Particle Physics, Physikalisches Institut,*

Universität Tübingen, D-72076 Tübingen, Germany

⁹*Department of Physics, University of Massachusetts Dartmouth, Dartmouth, MA 02747, USA*

(Dated: October 10, 2018)

Elastic scattering of photons from ^{12}C has been investigated using quasi-monoenergetic tagged photons with energies in the range 65 – 115 MeV at laboratory angles of 60° , 120° , and 150° at the Tagged-Photon Facility at the MAX IV Laboratory in Lund, Sweden. A phenomenological model was employed to provide an estimate of the sensitivity of the $^{12}\text{C}(\gamma, \gamma)^{12}\text{C}$ cross section to the bound-nucleon polarizabilities.

PACS numbers: 25.20.Dc

Keywords: Compton Scattering; Carbon; Polarizabilities.

I. INTRODUCTION

Much effort has been devoted to studying α and β , the electromagnetic polarizabilities of the proton and neutron. These polarizabilities represent the first-order responses of the internal structure of the nucleon to an external electric or magnetic field. The majority of nucleon-polarizability measurements have utilized the process of nuclear Compton scattering. A review of these experiments can be found in Ref. [1].

The most recent global fit [1] to all the data up to

170 MeV has yielded polarizabilities for the proton in units of 10^{-4} fm^3 of

$$\begin{aligned}\alpha_p &= 10.7 \pm 0.3_{\text{stat}} \pm 0.2_{\text{BSR}} \pm 0.8_{\text{th}} \\ \beta_p &= 3.1 \mp 0.3_{\text{stat}} \pm 0.2_{\text{BSR}} \pm 0.8_{\text{th}},\end{aligned}\quad (1)$$

where the first uncertainty is statistical, the second is due to uncertainties in the Baldin Sum Rule (BSR), and the third is due to theoretical uncertainty. The Baldin Sum Rule is given by [2]

$$\alpha + \beta = \frac{1}{2\pi^2} \int_{\omega_{\text{th}}}^{\infty} \frac{\sigma_\gamma(\omega) d\omega}{\omega^2}, \quad (2)$$

where $\sigma_\gamma(\omega)$ is the total photoabsorption cross section for the nucleon and ω_{th} is the threshold energy for pion photoproduction. These results were obtained under the constraint of the present-day evaluation [3] of the BSR for the proton which is

$$\alpha_p + \beta_p = 13.8 \pm 0.4. \quad (3)$$

Similarly, the neutron polarizabilities have been extracted from measurements of $^2\text{H}(\gamma, \gamma)^2\text{H}$. They have been determined to be

$$\begin{aligned}\alpha_n &= 11.1 \pm 1.8_{\text{stat}} \pm 0.4_{\text{BSR}} \pm 0.8_{\text{th}} \\ \beta_n &= 4.1 \mp 1.8_{\text{stat}} \pm 0.4_{\text{BSR}} \pm 0.8_{\text{th}}\end{aligned}\quad (4)$$

preserving the BSR for the neutron [4]

$$\alpha_n + \beta_n = 15.2 \pm 0.4. \quad (5)$$

*Present address: Thomas Jefferson National Accelerator Facility, Newport News, VA 23606, USA

†Present address: European Center for Theoretical studies in Nuclear Physics and Related Areas, Strada delle Tabarelle 286, I-38123 Villazzano, Trento, Italy

‡Present address: Department of Physics, University of Maryland, College Park, MD 20742, USA

§Corresponding author; kevin.fissum@nuclear.lu.se

¶Present address: National Security Technologies, Andrews AFB, MD 20762, USA

**Present Address: Trident Training Facility, Navy Submarine Base, Bangor, WA 98383, USA

††Present address: Institut für Kernphysik, University of Mainz, D-55128 Mainz, Germany

‡‡Present Address: LOASIS Program, Lawrence Berkeley National Lab, Berkeley, CA 94720, USA

§§Present address: Pacific Northwest National Laboratory, Richland, WA 99352, USA

TABLE I: Summary of nuclei studied using Compton scattering below the energy threshold for pion production.

Nucleus	Reference
^4He	[5], [6], [7]
^6Li	[8]
^{12}C	[9], [10], [11], [12], [13]
^{16}O	[7], [8], [11], [12], [14], [15]
^{40}Ca	[7], [9]

It is also reasonable to ask whether the nucleon polarizabilities are modified when the proton or neutron is bound in a nucleus and, if so, to what degree. A multitude of Compton-scattering experiments have been carried out with a variety of light nuclei (see Table I) for the purpose of determining the bound-nucleon polarizabilities (α_{eff} and β_{eff}) given by

$$\alpha_{\text{eff}} = \alpha_N + \Delta\alpha, \quad \beta_{\text{eff}} = \beta_N + \Delta\beta, \quad (6)$$

where α_N and β_N are the nucleon-averaged free polarizabilities and $\Delta\alpha$ and $\Delta\beta$ represent the nuclear modifications [13] which can be extracted from the scattering data.

These data sets have been analyzed using a model that parametrizes the Compton-scattering amplitude in terms of the photoabsorption cross section, its multipole decomposition and the bound-nucleon polarizabilities. The results typically produce a value for $\alpha_{\text{eff}} + \beta_{\text{eff}}$ that is in agreement with the free-nucleon sum rules given above [16]. However, though the sum is unchanged, several measurements [6, 15] have reported a significant modification to the electric polarizability ($\Delta\alpha$ approximately -5 to -10) whereas other groups report bound and free polarizabilities that are nearly equal [12]. In this paper we present a substantial new data set for Compton scattering from ^{12}C and report on the extracted values of the bound-nucleon polarizabilities.

II. PHENOMENOLOGICAL MODEL

A phenomenological model has been used to evaluate the sensitivity of the ^{12}C Compton-scattering data to the magnitude of the electromagnetic polarizabilities. This model is based on the work presented in [9]. The Compton-scattering amplitude can be written [15] in terms of the one- and two-body seagull (SG) amplitudes (which are explicitly dependent on the polarizabilities α_{eff} and β_{eff}) as

$$R(E, \theta) = R^{GR}(E, \theta) + R^{QD}(E, \theta) + R_1^{SG}(E, \theta) + R_2^{SG}(E, \theta). \quad (7)$$

The first two terms in Eq. 7 are related to the giant resonances ($E1$, $E2$, and $M1$; hereafter referred to as GR)

and the quasideuteron (QD) processes, respectively. The amplitudes are given by

$$R^{GR}(E, \theta) = f_{E1}(E)g_{E1}(\theta) + f_{E2}(E)g_{E2}(\theta) + f_{M1}(E)g_{M1}(\theta) + \frac{NZ}{A}r_0[1 + \kappa_{GR}]g_{E1}(\theta), \quad (8)$$

and

$$R^{QD}(E, \theta) = \left[f_{QD}(E) + \frac{NZ}{A}r_0\kappa_{QD} \right] \times F_2(q)g_{E1}(\theta), \quad (9)$$

where the complex forward-scattering amplitudes are denoted by $f_\lambda(E)$ ($\lambda = E1, E2, M1$), the appropriate angular factor is $g_\lambda(\theta)$ (see Ref. [8] for the angular factors), r_0 is the classical nucleon radius, and the enhancement factors $[1 + \kappa_{GR}]$ and κ_{QD} are the integrals of the GR and QD photoabsorption cross sections in units of the classical dipole sum rule. Since the QD process is modeled as an interaction with a neutron-proton pair, it is modulated by a two-body form factor $F_2(q)$ where q is the momentum transfer.

The seagull amplitudes account for subnucleon and meson-exchange degrees of freedom and are necessary to preserve gauge invariance in the total scattering amplitude. The one-body seagull amplitude is

$$R_1^{SG}(E, \theta) = \left\{ \left[-Zr_0 + \left(\frac{E}{\hbar c} \right)^2 A\alpha_{\text{eff}} \right] g_{E1}(\theta) + \left[\left(\frac{E}{\hbar c} \right)^2 A\beta_{\text{eff}} \right] g_{M1}(\theta) \right\} F_1(q), \quad (10)$$

where the higher-order terms have been omitted. This process is modulated by the one-body form factor $F_1(q)$ which is given by

$$F_1(q) = \frac{4\pi}{q} \int_0^\infty \rho(r) \sin(qr) r dr, \quad (11)$$

where $\rho(r)$ is given by the three-parameter Fermi function [17]

$$\rho(r) = \rho_0 \frac{1 + \frac{wr^2}{c^2}}{1 + e^{\frac{r-c}{z}}}, \quad (12)$$

with $w = -0.149$, $c = 2.355$ fm, $z = 0.522$ fm, and the form factor is normalized so that $F_1(0) = 1$.

The two-body seagull amplitude is

$$R_2^{SG}(E, \theta) = \left\{ \left[-\frac{NZ}{A}\kappa r_0 + \left(\frac{E}{\hbar c} \right)^2 A\alpha_{\text{ex}} \right] g_{E1}(\theta) + \left[\left(\frac{E}{\hbar c} \right)^2 A\beta_{\text{ex}} \right] g_{M1}(\theta) \right\} F_2(q), \quad (13)$$

where the exchange polarizabilities are denoted by α_{ex} and β_{ex} , $\kappa = \kappa_{GR} + \kappa_{QD}$, and the higher-order terms

TABLE II: $E2$, $M1$, and QD parameters.

Resonance	E_λ (MeV)	σ_λ (mb)	Γ_λ (MeV)
$E2$	26.0	1.8	0.50
	32.3	1.2	2.60
$M1$	15.1	29780	37×10^{-6}
QD	40	1.0	100

have been dropped. The two-body form factor is chosen by convention as $F_2(q) = [F_1(q/2)]^2$.

The parametrization of the $E1$ resonance is taken from Ref. [9] where the angle-averaged differential cross section was used to extract the $E1$ resonance below 40 MeV. The $E2$ strength between 25 and 35 MeV [12] and an $M1$ resonance [18] were also included. These included resonances are listed in Table II.

Levinger's modified quasideuteron model [19] and a damped Lorentzian lineshape were used to define a piecewise function to parametrize the QD process (Eq. 14). This parametrization was fitted to the existing total photoabsorption cross-section data [20] above 50 MeV in order to establish the normalization. The QD scattering cross section was taken to be

$$\sigma_{QD}(E) = \begin{cases} \frac{1}{2} [1 + \tanh \frac{E-E_t}{\Delta E}] \mathcal{L}_{QD}(E) & : E < 50 \text{ MeV} \\ L e^{-D/E} [\frac{NZ}{A}] \sigma_D(E) & : E > 50 \text{ MeV,} \end{cases} \quad (14)$$

where $\sigma_D(E)$ is the deuteron photoabsorption cross section and the parameters $L = 5.0$ and $D = 5.4$ were determined from the fit to the data. The Lorentzian $\mathcal{L}_{QD}(E)$ has the parameters E_{QD} , Γ_{QD} , and σ_{QD} given in Table II, with $E_t = 40$ MeV and $\Delta E = 10$ MeV. Since the analysis of Warkentin *et al.* [13] indicated that the extraction of α_{eff} and β_{eff} depends only slightly on the parametrization of the QD amplitude, only the above parametrization will be used in this analysis.

III. EXPERIMENT

The experiment was performed at the Tagged-Photon Facility [21, 22] located at the MAX IV Laboratory [23] in Lund, Sweden. A pulse-stretched electron beam [24] with nominal energies of 144 MeV and 165 MeV, a current of 15 nA, and a duty factor of 45% was used to produce quasi-monoenergetic photons in the energy range 65 – 115 MeV via the bremsstrahlung-tagging technique [25, 26]. An overview of the experimental layout is shown in Fig. 1.

The size of the photon beam was defined by a tapered tungsten-alloy primary collimator of 19 mm nominal diameter. The primary collimator was followed by a dipole magnet and a post-collimator which were used to remove any charged particles produced in the primary collimator.

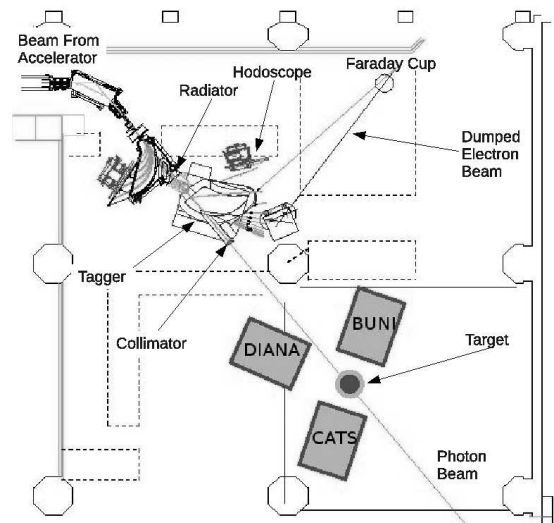


FIG. 1: The layout of the experimental area showing the location of the focal-plane hodoscope, ^{12}C target, and NaI(Tl) detectors labeled DIANA, BUNI, and CATS.

The beam spot at the target location was approximately 60 mm in diameter.

The tagging efficiency [26] is the ratio of the number of tagged photons which struck the target to the number of post-bremsstrahlung electrons which were registered by the associated focal-plane channel. It was measured absolutely during the experiment startup with three large-volume NaI(Tl) photon spectrometers placed directly in the beam (see below) and it was monitored during the experiment itself on a daily basis using a lead-glass photon detector. The tagging efficiency was determined to be $(44 \pm 1)\%$ throughout the experiment.

A graphite block 5.22 cm thick was used as a target. The density of the target was measured to be $(1.83 \pm 0.02) \text{ g/cm}^3$. The target was positioned such that the photon beam was perpendicular to the face of the target resulting in a target thickness of $(4.80 \pm 0.07) \times 10^{23}$ nuclei/cm². The average loss of incident photon-beam flux due to absorption in the target was approximately 7%.

Three large-volume, segmented NaI(Tl) detectors labeled BUNI [27], CATS [28], and DIANA [29] in Fig. 1 were used to detect the Compton-scattered photons. The detectors were located at laboratory angles of 60° , 120° , and 150° . These detectors were each composed of a single, large NaI(Tl) crystal surrounded by optically-isolated, annular NaI(Tl) segments. The detectors have an energy resolution of better than 2% at energies near 100 MeV. Such resolution is necessary to unambiguously separate elastically scattered photons from those originating from the breakup of deuterium, a parallel and ongoing experimental effort to be reported upon in the near future.

IV. DATA ANALYSIS

A. Yield Extraction

The signals from each detector were passed to analog-to-digital converters (ADCs) and time-to-digital converters (TDCs) and the data recorded on an event-by-event basis. The comprehensive dataset presented in this paper was acquired over a five-year period from 2007 to 2012. During this time, the single-hit TDCs used to instrument the tagger focal plane were complemented with multi-hit TDCs. Data obtained using both types of TDCs are presented here ¹. The ADCs allowed reconstruction of the scattered-photon energies, while the TDCs enabled coincident timing between the NaI(Tl) detectors and the focal-plane hodoscope. The energy calibration of each detector was determined by placing them directly into the photon beam and observing their response as a function of tagged-photon energy. A typical measured in-beam lineshape together with a **GEANT4** simulation [32] of the response function of the detector fitted to the data is shown in Fig. 2.

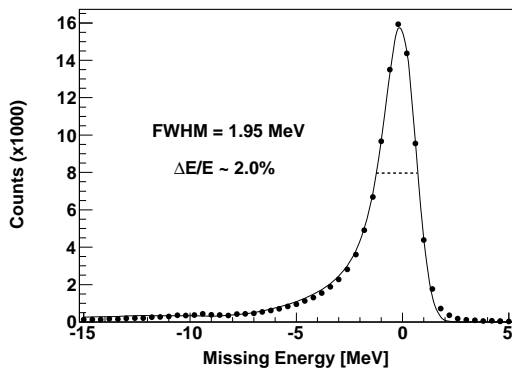


FIG. 2: Typical in-beam detector response to incident photons as a function of missing energy. The curve is the simulated **GEANT4** detector response fitted to the data.

Large backgrounds arose when the detectors were moved to the various scattering angles and the beam intensity was increased from 10-100 Hz (for in-beam runs) to 1-4 MHz. Untagged bremsstrahlung photons (related to the beam intensity) and cosmic rays (constant) were the dominant sources of background. An energy cut that accepted only events in the tagged-energy range enabled the prompt peak (representing coincidences between electrons in the focal-plane hodoscope and events in the NaI(Tl) detectors) to be identified in the focal-plane TDC spectra (see Fig. 3). For each NaI(Tl) de-

tor, events occurring within the prompt peak were selected and a prompt missing-energy (ME) spectrum was filled. ME was defined as the difference between the detected photon energy and the expected photon energy based upon the tagged-electron energy. A second cut was placed on an accidental (or random) timing region and an accidental ME spectrum was filled. This process was carried out for each focal-plane channel.

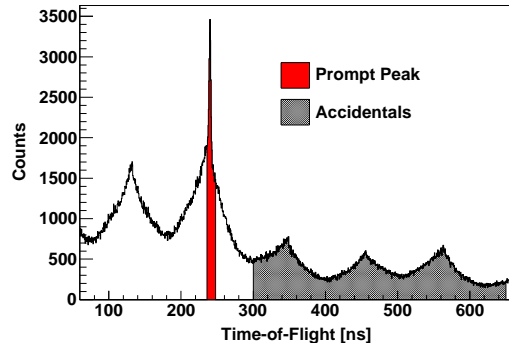


FIG. 3: (Color online) The focal-plane TDC spectrum for the scattering data. The prompt (red) and the accidental (grey) windows are indicated.

A net sum ME spectrum for each focal-plane channel was generated by removing both the cosmic-ray and untagged-photon backgrounds. Due to the complex nature of the time structure that exists in the focal-plane TDC spectrum, this process was carried out in two steps. First, the cosmic-ray contribution was subtracted from both the prompt and accidental ME spectra by normalizing these spectra in the energy region above the electron-beam energy. Next, the cosmic-subtracted accidentals were removed from the cosmic-subtracted prompts by normalizing the two spectra in the energy range above the tagged-photon energy corresponding to the particular focal-plane channel but below the electron-beam energy. The focal plane was divided into 4 energy bins, each approximately 9 MeV wide. The background-corrected ME spectrum for each tagged channel in a particular energy bin was then summed to create a ME spectrum for that bin, such as the one shown in Fig. 4.

A **GEANT4** simulation was employed to determine the total yield in the elastic-scattering peak and also to quantify any corrections due to finite geometrical effects. The simulation output was first determined for the case of a NaI(Tl) detector positioned directly in the low-intensity photon beam ($\theta=0^\circ$) as shown in Fig. 2. This intrinsic simulation was then smeared with a Gaussian function to phenomenologically account for the individual characteristics of each NaI(Tl) detector that are difficult to model in **GEANT4**. The simulated detector response, with the smearing determined as above, was then fitted to the scattering data over the region of interest (ROI) indicated by the vertical dashed lines shown in Fig. 4. The fitted **GEANT4** lineshape was then used to correct for the

¹ The interested reader is directed to Refs. [30, 31] for a detailed discussion and comparison of the results obtained using the two different types of TDCs.

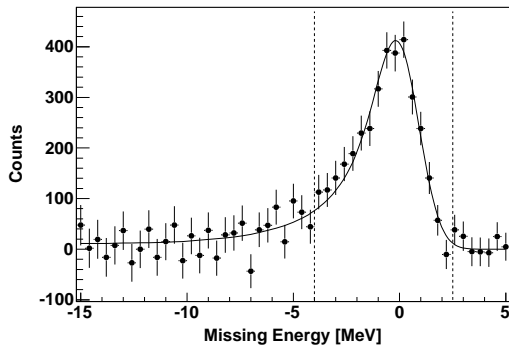


FIG. 4: A typical missing-energy spectrum for a focal-plane bin obtained in one of the scattering configurations, with both cosmics and accidentals removed. The solid line is the fit of the `GEANT4` lineshape to the data. The dashed lines indicate the ROI used to determine the yield of Compton-scattered photons (see text).

detection efficiency of the NaI(Tl) detector in the ROI. This efficiency accounts for events that deposit some energy outside the ROI in the detector. Additionally, the correction factor for photons absorbed by the target and the correction to the detector acceptance due to the finite geometry of the experimental setup were obtained from this simulation.

B. Normalization

The scattering-photon yield was then normalized to the number of photons incident on the target and corrected for rate-dependent factors. The number of photons incident on the target was determined from the number of post-bremsstrahlung electrons detected in each focal-plane channel and the measured tagging efficiency. The rate-dependent corrections included “stolen” trues [33], “missed” trues, and “ghost” events [34]. A stolen true arose when a random electron was detected in the focal-plane channel prior to the electron corresponding to the tagged photon. This correction was only applied to the single-hit TDC data. It was determined using the method outlined in Ref. [35] and was typically 20 – 45%. Missed trues resulted from deadtime effects in the focal-plane instrumentation electronics. Ghost events were an artifact of the physical overlap of the focal-plane counters. The missed-trues and ghost corrections were determined using a Monte Carlo simulation of the focal-plane electronics and amounted to approximately 5% and 1%, respectively².

² The interested reader is directed to Ref. [30] for a detailed discussion of the focal-plane simulation.

TABLE III: Systematic uncertainties.

Type	Variable	Value
Scale	Tagging Efficiency	~1%
	Target Thickness	~1%
	Missed Trues	~1%
	Ghost Events	~2%
Angular	Detector Acceptance	3–4%
Point-to-Point	Stolen Trues	2–4%
Total		5–7%

C. Systematic Uncertainties

The systematic uncertainties in this experiment were grouped into three types. The first was an overall scale systematic uncertainty that affected the data obtained at all angles and energies equally. This uncertainty arose from normalization factors such as the tagging efficiency. The second type of uncertainty varied only with angle but not energy and was due to the acceptance of the individual NaI(Tl) detectors. This uncertainty had two origins: (1) the distance and aperture size of the detector in its scattering location; and (2) the effect of placing cuts on the data during analysis. Finally, certain uncertainties were strongly dependent on kinematics and varied with both energy and angle such as the stolen-trues correction. The dominant sources of systematic uncertainties are listed in Table III along with typical values. The systematic uncertainties were combined in quadrature to obtain the overall systematic uncertainty.

D. Cross Sections

The ^{12}C elastic scattering cross sections measured in this experiment are presented in Table IV. The results are also shown in Fig. 5, along with the results from [10–13] above 55 MeV. The new data are in excellent agreement with the results from Schelhaas *et al.* [10] and Warkentin *et al.* [13].

V. RESULTS

The most recent interpretations of $^{12}\text{C}(\gamma,\gamma)$ cross-section data [12, 13] utilize multiple Lorentzian lineshapes to construct the $E1$ scattering amplitude. However, in our analysis, the phenomenological model is unable to fit the low-energy data of Wright *et al.* [9] using these lineshapes (see Fig. 6). In an attempt to incorporate all the published data, we have elected to use the analysis procedure detailed in [9] where the $E1$ resonance is deduced from the low-energy (≤ 40 MeV), angle-averaged Compton-scattering cross section, and the QD scattering amplitude is given by Eq. 14. The $E2$ and $M1$ resonances below 40 MeV are included for completeness, but have little effect on the results.

TABLE IV: Measured cross sections for $^{12}\text{C}(\gamma, \gamma)$ at the lab angles listed. The type of TDC used to record coincidences is indicated. The first uncertainty is statistical and the second uncertainty is total systematic.

E_γ (MeV)	$\frac{d\sigma}{d\Omega}(60^\circ)$ (nb/sr)	$\frac{d\sigma}{d\Omega}(120^\circ)$ (nb/sr)	$\frac{d\sigma}{d\Omega}(150^\circ)$ (nb/sr)
Single-hit TDCs, $E_{\text{beam}} = 144$ MeV			
69.6		$618 \pm 24 \pm 42$	$599 \pm 28 \pm 32$
77.9		$502 \pm 19 \pm 32$	$496 \pm 24 \pm 26$
86.1		$423 \pm 17 \pm 26$	$354 \pm 21 \pm 18$
93.4		$354 \pm 16 \pm 23$	$298 \pm 23 \pm 16$
Single-hit TDCs, $E_{\text{beam}} = 165$ MeV			
85.8	$439 \pm 29 \pm 29$	$519 \pm 21 \pm 34$	$389 \pm 21 \pm 22$
94.8	$312 \pm 24 \pm 19$	$358 \pm 16 \pm 23$	$284 \pm 17 \pm 18$
103.8	$261 \pm 21 \pm 17$	$309 \pm 15 \pm 20$	$230 \pm 14 \pm 13$
112.1	$233 \pm 19 \pm 16$	$223 \pm 12 \pm 15$	$156 \pm 13 \pm 9$
Multi-hit TDCs, $E_{\text{beam}} = 165$ MeV			
87.3	$389 \pm 14 \pm 16$	$365 \pm 11 \pm 14$	$381 \pm 11 \pm 14$
96.3	$324 \pm 13 \pm 13$	$312 \pm 10 \pm 13$	$312 \pm 10 \pm 13$
104.7	$212 \pm 11 \pm 11$	$256 \pm 8 \pm 11$	$263 \pm 8 \pm 13$
112.9	$209 \pm 9 \pm 10$	$213 \pm 7 \pm 10$	$166 \pm 7 \pm 8$
Single-hit TDCs, $E_{\text{beam}} = 165$ MeV			
65.5	$562 \pm 42 \pm 35$	$570 \pm 22 \pm 29$	
75.7	$470 \pm 28 \pm 29$	$519 \pm 17 \pm 25$	
86.2	$392 \pm 27 \pm 22$	$398 \pm 16 \pm 18$	
95.9	$281 \pm 23 \pm 14$	$294 \pm 15 \pm 13$	
Multi-hit TDCs, $E_{\text{beam}} = 165$ MeV			
65.5	$517 \pm 34 \pm 22$	$546 \pm 19 \pm 24$	
75.7	$432 \pm 23 \pm 18$	$489 \pm 15 \pm 20$	
86.2	$368 \pm 22 \pm 16$	$372 \pm 14 \pm 15$	
95.9	$250 \pm 20 \pm 10$	$300 \pm 14 \pm 12$	

As suggested by Wright *et al.* [9] and reinforced by Warkentin *et al.* [13], we also allowed for the possibility of E2 strength above 50 MeV. A third E2 resonance was added to the phenomenological model (with an equivalent lineshape subtracted from the QD parametrization so as to not affect the total photoabsorption cross section [14]) with a width of 30 MeV. The best fits to the data were achieved with an E2 resonance energy of approximately 90 MeV and a peak strength of approximately 0.2 mb. These values are consistent with the resonance assumed by Warkentin *et al.* The addition of this E2 resonance reduced χ^2 by approximately 30% compared to an identical fit without the additional E2 strength.

With the above parametrization, we were able to fit the entire world data set (excluding the data from Hager *et al.* [12]) below 150 MeV with the phenomenological model. Four different approaches were used involving different combinations of the BSR, the bound-nucleon polarizabilities (α_{eff} and β_{eff}), and the exchange polarizabilities (α_{ex} and β_{ex}) (see Table V). In approach (1), α_{eff} and β_{eff} were varied under the BSR constraint while

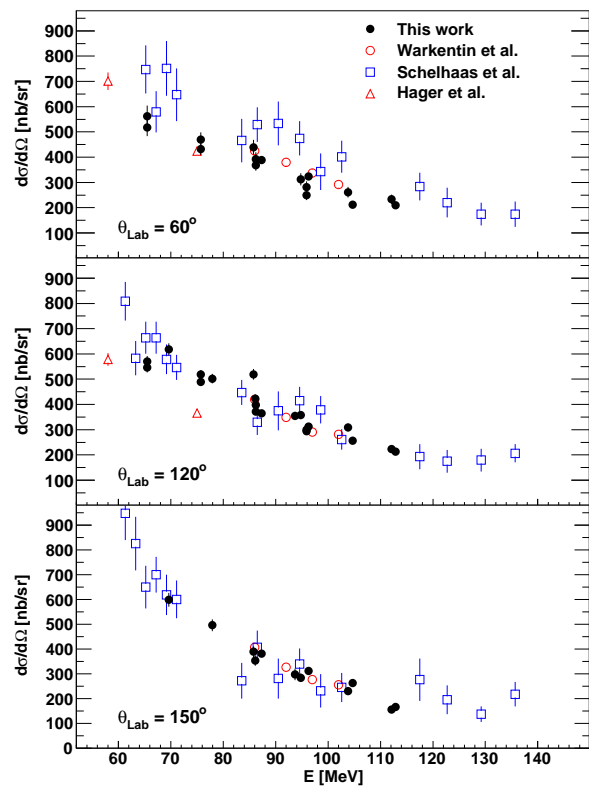


FIG. 5: (Color online) Measurements of the ^{12}C Compton-scattering cross section from previous experiments compared to the results from the current experiment. Statistical uncertainties are shown.

$\alpha_{\text{ex}} = \beta_{\text{ex}} = 0$ were fixed. In approach (2), the effective polarizabilities were fixed while the exchange polarizabilities were varied. In approach (3), $\alpha_{\text{ex}} = \beta_{\text{ex}} = 0$ were once again fixed, and α_{eff} and β_{eff} were varied without the BSR constraint. In approach (4), using only the BSR constraint, all the polarizabilities were allowed to vary in order to minimize the χ^2/DOF . In all four cases, the additional E2 resonance was fixed at $E_{\text{res}} = 89$ MeV, $\sigma_{\text{res}} = 0.22$ mb, and $\Gamma_{\text{res}} = 30$ MeV) as minor variations in the resonance parameters had a negligible effect on the results. Together with the E1 parametrization developed by Wright *et al.* [9], this analysis presents a consistent framework for fitting the scattering data from photon energies below the giant dipole resonance to energies near the threshold for pion production. The results are summarized in Table V (quantities listed without uncertainties were held fixed during the fitting) and are shown in Fig. 7.

The extracted value of α_{eff} varied over the range 3–11. Additionally, the exchange polarizabilities were quite large depending on the values used for α_{eff} and β_{eff} . Thus, it is clear that this model for Compton scattering is unable to differentiate between in-medium modifications to the free-nucleon polarizabilities and the effects of the two-body exchange polarizabilities. The results of

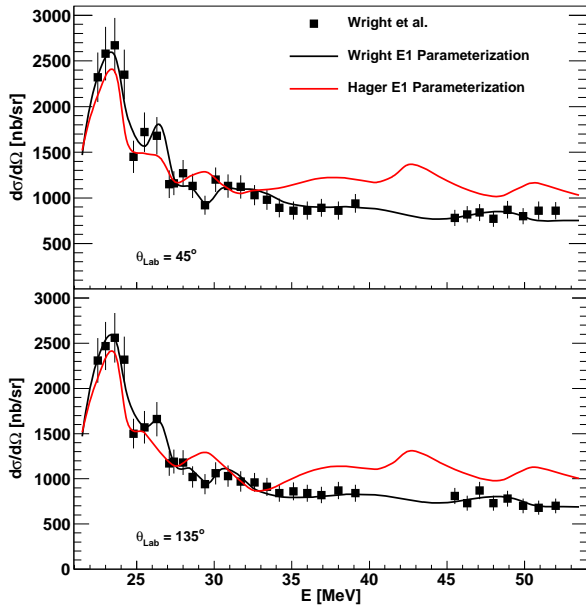


FIG. 6: (Color online) Comparison of the fit to the Wright *et al.* data [9] using the $E1$ resonance parametrization suggested by the author (black) as well as that of Häger *et al.* [12] (red).

TABLE V: Extracted values of the effective and exchange polarizabilities subject to the constraints outlined in the text.

approach	$\alpha_{\text{eff}} + \beta_{\text{eff}}$	α_{eff}	β_{eff}	α_{ex}	β_{ex}
(1)	14.5	3.4 (0.2)	11.1 (0.2)	0	0
(2)	14.5	10.9	3.6	-3.9 (0.2)	6.4 (0.2)
(3)	18.3 (0.3)	4.9 (0.2)	13.4 (0.2)	0	0
(4)	14.5	3.6 (1.1)	10.9 (1.1)	1.3 (0.8)	2.1 (0.7)

our analysis indicate that the net electric polarizability of the bound nucleon ($\alpha_{\text{eff}} + \alpha_{\text{ex}}$) is significantly reduced from its free value and that the magnetic polarizability is much larger than its free value. This is in direct opposition to the results reported by Häger *et al.* [12] where the observed bound-nucleon polarizabilities were in agreement with the free values. The sources of this discrepancy are the reported cross sections, especially at the backward scattering angles (see Fig. 5), and the choice of the model parametrization. Fitting the Häger *et al.* [12] data alone with the model developed in this paper (with $\alpha_{\text{ex}} = \beta_{\text{ex}} = 0$ fixed) produces a value of $\alpha_{\text{eff}} = 8.2 \pm 0.5$ and $\beta_{\text{eff}} = 6.3 \mp 0.5$. Thus, the choice of the resonance parametrization explains part of the discrepancy. We note that the Häger *et al.* [12] cross-section data, especially at the backward angles, are much smaller than those reported in most other experiments [10, 11, 13]. The effect of a smaller cross section is an increase in the difference $\alpha_{\text{eff}} - \beta_{\text{eff}}$ which, in turn, produces values for the bound polarizabilities much closer to their free values. Based on our data and the analysis presented here, we

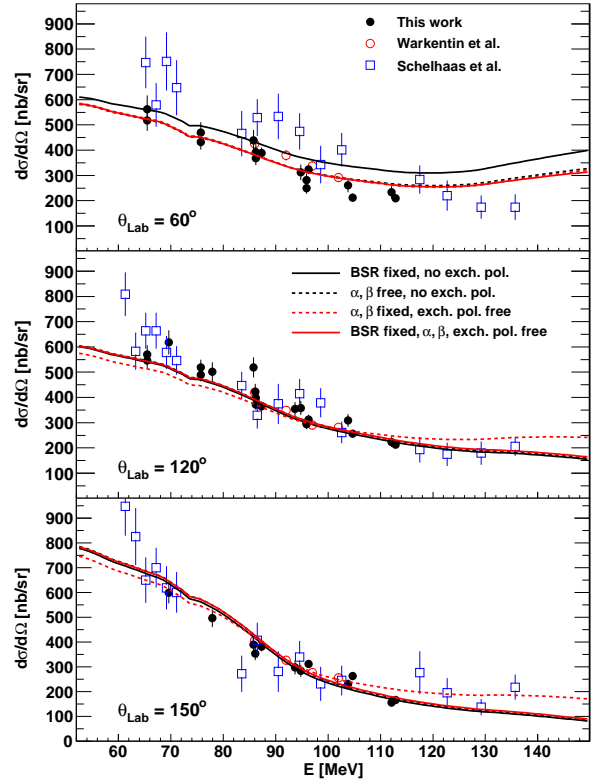


FIG. 7: (Color online) Comparison of the fits to the data obtained by varying $\alpha_{\text{eff,ex}}$ and $\beta_{\text{eff,ex}}$ as described in the text. The uncertainties shown are the statistical and systematic uncertainties added in quadrature.

assert that either the bound-nucleon polarizabilities differ considerably from the free-nucleon values or there are substantial contributions of two-body exchange polarizabilities. Both of these statements agree with the conclusions of Feldman *et al.* [15] drawn based upon $^{16}\text{O}(\gamma, \gamma)$ data.

VI. CONCLUSIONS

In this work, we present a new measurement of the ^{12}C Compton-scattering cross section for the energy range 65–115 MeV. The results are in good agreement with the previously published results of Schelhaas *et al.* [10], Ludwig *et al.* [11], and Warkentin *et al.* [13]. However, there is a substantial discrepancy with the results reported by Häger *et al.* [12].

The values of the extracted bound-nucleon polarizabilities were found to be strongly dependent on the parametrization of the cross section. The range of extracted α_{eff} was 3–11 depending on whether or not the exchange polarizabilities were included. Based on the results and analysis, there are in-medium effects and/or exchange polarizabilities that must be accounted for in a full calculation of the Compton-scattering process. Un-

fortunately, the current world-data set does not indicate which of these effects is more important. The data do seem to have a strong preference for additional $E2$ strength located above 50 MeV which could be experimentally determined.

Acknowledgments

The authors acknowledge the outstanding support of the staff of the MAX IV Laboratory which made this experiment successful. We also gratefully acknowledge the Data Management and Software Centre, a Dan-

ish contribution to the European Spallation Source ESS AB, for generously providing access to their computations cluster. The Lund group acknowledges the financial support of the Swedish Research Council, the Knut and Alice Wallenberg Foundation, the Crafoord Foundation, the Swedish Institute, the Wenner-Gren Foundation, and the Royal Swedish Academy of Sciences. This work was sponsored in part by the U.S. Department of Energy under grants DE-FG02-95ER40901, DE-FG02-99ER41110, and DE-FG02-06ER41422, the US National Science Foundation under Award Number 0853760 and the UK Science and Technology Facilities Council.

-
- [1] H.W. Griebhammer, J.A. McGovern, D.R. Phillips, and G. Feldman, *Prog. Part. Nucl. Phys.* **67**, 841 (2012).
- [2] A.M. Baldin, *Nucl. Phys.* **18**, 310 (1960).
- [3] V. Olmos de León, F. Wissmann, P. Achenbach, J. Ahrens, H.-J. Arends, R. Beck, P.D. Harty, V. Hejny, P. Jennewein, M. Kotulla, et al., *Eur. Phys. J. A* **10**, 207 (2001).
- [4] M.I. Levchuk and A.I. L'vov, *Nucl. Phys. A* **674**, 449 (2000).
- [5] D.P. Wells, Ph.D. thesis, University of Illinois at Urbana-Champaign, Champaign, IL, USA (1990).
- [6] K. Fuhrberg, D. Häger, T. Glebe, B.-E. Andersson, K. Hansen, M. Hütt, B. Nilsson, L. Nilsson, D. Ryckbosch, B. Schröder, et al., *Nucl. Phys. A* **591**, 1 (1995).
- [7] S. Proff, C. Pösch, T. Glebe, J.-O. Adler, K. Fissum, K. Hansen, M.-Th. Hütt, O. Kaltschmidt, M. Lundin, B. Nilsson, et al., *Nucl. Phys. A* **646**, 67 (1999).
- [8] L.S. Myers, M.W. Ahmed, G. Feldman, S.S. Henshaw, M.A. Kovash, J.M. Mueller, and H.R. Weller, *Phys. Rev. C* **86**, 044614 (2012).
- [9] D.H. Wright, P.T. Debevec, L.J. Morford, and A.M. Nathan, *Phys. Rev. C* **32**, 1174 (1985).
- [10] K.P. Schelhaas, J.M. Henneberg, N. Wieloch-Laufenberg, U. Zurmühl, B. Ziegler, M. Schumacher, and F. Wolf, *Nucl. Phys. A* **506**, 307 (1990).
- [11] M. Ludwig, B.-E. Andersson, A. Baumann, K.I. Blomqvist, K. Fuhrberg, E. Hayward, G. Müller, D. Nilsson, A. Sandell, B. Schröder, et al., *Phys. Lett. B* **274**, 275 (1992).
- [12] D. Häger, K. Fuhrberg, T. Glebe, M. Hütt, M. Ludwig, M. Schumacher, B.-E. Andersson, K. Hansen, B. Nilsson, B. Schröder, et al., *Nucl. Phys. A* **595**, 287 (1995).
- [13] B. J. Warkentin, D. L. Hornidge, R. Igarashi, J. C. Bergstrom, E. L. Hallin, N. R. Kolb, R. E. Pywell, D. M. Skopik, J. M. Vogt, and G. Feldman, *Phys. Rev. C* **64**, 014603 (2001).
- [14] K.E. Mellendorf, Ph.D. thesis, University of Illinois at Urbana-Champaign, Champaign, IL, USA (1993).
- [15] G. Feldman, K.E. Mellendorf, R.A. Eisenstein, F.J. Federspiel, G. Garino, R. Igarashi, N.R. Kolb, M.A. Lucas, B.E. MacGibbon, W.K. Mize, et al., *Phys. Rev. C* **54**, 2124 (1996).
- [16] M.-Th. Hütt, A.I. L'vov, A.I. Milstein, and M. Schumacher, *Phys. Reports* **323**, 457 (2000).
- [17] C.W. de Jager, H. D. Vries, and C. D. Vries, *At. Data Nucl. Data Tables* **14**, 479 (1974).
- [18] E. Hayward, in *Giant Multipole Resonances*, edited by S. Costa and C. Schaerf (Springer-Verlag, Berlin, 1977), p. 340.
- [19] J.S. Levinger, *Phys. Lett.* **B82**, 181 (1979).
- [20] J. Ahrens, H. Borchert, K.H. Czock, H.B. Eppler, H. Gimm, H. Gundrum, M. Kröning, P. Riehn, G. S. Ram, A. Zieger, et al., *Nucl. Phys.* **A251**, 479 (1975).
- [21] <https://www.maxlab.lu.se/node/1090>.
- [22] J.-O. Adler, M. Boland, J. Brudvik, K. Fissum, K. Hansen, L. Isaksson, P. Lilja, L.-J. Lindgren, M. Lundin, B. Nilsson, et al., *Nucl. Instrum. Methods Phys. Res. Sect. A* **715**, 1 (2013).
- [23] <https://www.maxlab.lu.se>.
- [24] L.-J. Lindgren, *Nucl. Instrum. Methods Phys. Res. Sect. A* **492**, 299 (2002).
- [25] J.-O. Adler, B.-E. Andersson, K. I. Blomqvist, B. Forkman, K. Hansen, L. Isaksson, K. Lindgren, D. Nilsson, A. Sandell, B. Schröder, et al., *Nucl. Instrum. Methods Phys. Res. Sect. A* **294**, 15 (1990).
- [26] J.-O. Adler, B.-E. Andersson, K. I. Blomqvist, K. G. Fissum, K. Hansen, L. Isaksson, B. Nilsson, D. Nilsson, H. Ruijter, A. Sandell, et al., *Nucl. Instrum. Methods Phys. Res. Sect. A* **388**, 17 (1997).
- [27] J.P. Miller, E.J. Austin, E.C. Booth, K.P. Gall, E.K. McIntyre, and D.A. Whitehouse, *Nucl. Instrum. Methods Phys. Res. Sect. A* **270**, 431 (1988).
- [28] F. Wissmann, V. Kuhr, O. Jahn, H. Vorwerk, P. Achenbach, J. Ahrens, H.-J. Arends, R. Beck, M. Camen, G. Caselotti, et al., *Nucl. Phys. A* **660**, 232 (1999).
- [29] L.S. Myers, Ph.D. thesis, University of Illinois at Urbana-Champaign, Champaign, IL, USA (2010).
- [30] L.S. Myers, G. Feldman, K.G. Fissum, L. Isaksson, M.A. Kovash, A.M. Nathan, R.E. Pywell, and B. Schröder, *Nucl. Instrum. Methods Phys. Res. Sect. A* **729**, 707 (2013).
- [31] M.F. Preston, L.S. Myers, J.R.M. Annand, K.G. Fissum, K. Hansen, L. Isaksson, R. Jebali, and M. Lundin, accepted for publication in *Nucl. Instrum. Methods Phys. Res. Sect. A* in 2014.
- [32] S. Agostinelli, *Nucl. Instrum. Methods Phys. Res. Sect. A* **506**, 250 (2003).
- [33] R.O. Owens, *Nucl. Instrum. Methods Phys. Res. Sect. A* **A288**, 574 (1990).
- [34] B.E. MacGibbon, Ph.D. thesis, University of Illinois at

- Urbana-Champaign, Champaign, IL, USA (1995).
- [35] L. V. Hoorebeke, D. Ryckbosch, C. V. den Abeele, R. V. de Vyver, J. Dias, F. D. Smet, B. Schröder, and D. Nilsson, Nucl. Instrum. Methods Phys. Res. Sect. A **A321**, 230 (1992).